

Spatio-temporal Variation of Water Heat Flux Using MODIS Land Surface Temperature Product over Hulun Lake, China During 2001–2018

ZHAO Boyu¹, DU Jia¹, SONG Kaishan¹, Pierre-André JACINTHE², XIANG Xiaoyun¹, ZHOU Haohao¹, YANG Zhichao³, ZHANG Liyan⁴, GUO Pingping⁵

(1. Northeast Institute of Geography and Agroecology, Chinese Academy of Sciences, Changchun 130102, China; 2. Department of Earth Sciences, Indiana University-Purdue University Indianapolis, IN 46202, USA; 3. University of Science and Technology Liaoning, Anshan 114051, China; 4. Jinan District Bureau of Natural Resources and Planning, Fuzhou 350002, China; 5. Minjiang River Estuary Wetland National Nature Reserve Administrative Office, Fuzhou 350002, China)

Abstract: Heat flux is important for studying interactions between atmosphere and lake. The heat exchange between air-water interfaces is one of the important ways to govern the temperature of the water surface. Heat exchange between the air-water interfaces and the surrounding environment is completed by solar radiation, conduction, and evaporation, and all these processes mainly occur at the air-water interface. Hulun Lake was the biggest lake which is also an important link and an indispensable part of the water cycle in Northeast China. This study mapped surface energy budget to better understand spatial and temporal variations in Hulun Lake in China from 2001 to 2018. Descriptive statistics were computed to build a historical time series of mean monthly heat flux at daytime and nighttime from June to September during 2001–2018. Remote sensing estimation methods we used was suitable for Hulun Lake ($R^2 = 0.81$). At month scale, shortwave radiation and latent heat flux were decrease from June to September. However, the maximum sensible heat flux appeared in September. Net longwave radiation was the largest in August. The effective heat budget showed that Hulun Lake gained heat in the frost-free season with highest value in June (686.31 W/m^2), and then steadily decreased to September (439.76 W/m^2). At annual scale, net longwave radiation, sensible heat flux and latent heat flux all show significant growth trend from 2001 to 2018 ($P < 0.01$). Wind speed had the well correlation on sensible heat flux and latent heat flux. Water surface temperature showed the highest coefficient in sensitivity analysis.

Keywords: water surface temperature (WST); heat flux; Moderate Resolution Imaging Spectroradiometer (MODIS); remote sensing; Hulun Lake, China

Citation: ZHAO Boyu, DU Jia, SONG Kaishan, Pierre-André JACINTHE, XIANG Xiaoyun, ZHOU Haohao, YANG Zhichao, ZHANG Liyan, GUO Pingping, 2020. Spatio-temporal Variation of Water Heat Flux Using MODIS Land Surface Temperature Product over Hulun Lake, China During 2001– 2018. *Chinese Geographical Science*, 30(6): 1065–1080. <https://doi.org/10.1007/s11769-020-1166-4>

1 Introduction

Over a couple of years, the impact of global climate change on humans has been observed and recorded

many times worldwide, especially the effects of global warming. Hulun Lake is one of lakes located in the arid and cold regions of northern China. It is an important link and an indispensable part of the water cycle in these

Received date: 2020-03-09; accepted date: 2020-07-01

Foundation item: Under the auspices of National Key Research and Development Program of China (No. 2016YFA0602301, 2016YFB0501502), Strategic Planning Project of the Northeast Institute of Geography and Agroecology (IGA), Chinese Academy of Sciences (No. Y6H2091001), National Forestry Science and Technology Demonstration Promotion Project (No. JLT2018-03)

Corresponding author: DU Jia. E-mail: jiaqidu@iga.ac.cn

© Science Press, Northeast Institute of Geography and Agroecology, CAS and Springer-Verlag GmbH Germany, part of Springer Nature 2020

regions (Wang et al., 2010). Studies have shown that owing to the warming and drying of the climate, the supply of water in Hulun Lake is decreasing, and has caused the level of water dropped, a shrinking of the surface of the lake, a large reduction in the surrounding reeds, the migration from the area of a large number of rare birds, and serious deterioration of the ecological environment (Mao, 2017).

In recent decades, the importance of changes in features of inland lakes, such as area and water level, to changes in climate and water cycle has been recognized (Zhang et al., 2011; Chen et al., 2016; Qiao et al., 2019). It can also help us understand global climate change in a broader context. An important feedback of a lake to climatic warming is the change of lake surface water temperature (LSWT). LSWT is one of the most fundamental drivers of ecosystem structure and function, which affects the rates and equilibrium positions of chemical reactions and the rates of metabolic processes. Moreover, the heat exchange between air-water interfaces is one of the important ways to govern the temperature of the water surface. Because the heat exchange between the air-water interfaces and the surrounding environment is completed by solar radiation, conduction, and evaporation, and all these processes mainly occur at the air-water interface (Woolway et al., 2016; Yang et al., 2019). The net rate of heat exchange at water surface is the sum of the rates at which heat is transferred by radiative processes, evaporation, and conduction between water and overlying air that govern water surface temperature. The net rate can be evaluated in terms of a thermal exchange coefficient and an equilibrium temperature, both of which depend on observable meteorological variables (Edinger et al., 1968). In addition, temperature difference between water and air also affects the heat exchange in the air-water boundary layer, which is crucial to understanding the hydrological cycle (Alcântara et al., 2011).

Heat flux is important for studying interactions between atmosphere and lake, and is also affected by warming over the northeastern China. Thermal cycling is usually triggered by huge thermal contrasts, which come from the lake and surrounding land. Thermal cycling often has serious effects on transportation and air pollution in lake basins. Storms in downwind areas will be intensified by large lakes because they are important sources of atmospheric moisture (Pour et al., 2017). In

addition of the periods of high algal movement (Bogard et al., 2017), water of lake is often saturated with Carbon Oxide than the atmosphere and plays as the source of carbon in the atmosphere (Cole et al., 1994). What's more, atmospheric CH_4 (Wang et al., 2019) and N_2O (Huttunen et al., 2003) also source from lake.

Traditionally, most analysis on the heat flux of lakes was based on *in-situ* measurements, which are dispersed and rarely collected from optimal locations (Hébert and Dunlop, 2020). In addition, it seems consuming time and expensive if the measurements are performed *in-situ* (Hodges et al., 2016). The data of heat flux and water temperature at high spatio-temporal resolutions are required for more utilizations, for example, the monitoring system for the changes of climate, research on the water quality management, aquaculture, fishery, habitats of aquatic organisms and hydrological cycle. Some researchers also used thermal infrared remote sensing in freshwater ecosystems to draw cyclic patterns (Schladow et al., 2004). Overall temperature (Alcântara et al., 2011) and surface dimensions (Xu et al., 2009; Sharaf et al., 2019; Viridis et al., 2020) and to mark the upwelling events (Steissberg et al., 2005).

However, little research has been devoted to the response of the thermal variables of lakes, specifically changes in the heat flux. The study area of this work, the Hulun Lake, was one of the representative freshwater lakes in temperate continental climate, which was the biggest lake in Northeast China and the fifth biggest fresh water lake in China (Mao, 2017). Based on meteorological data and remote sensing data, we reveal the spatial and temporal evolution patterns of heat flux using the heating exchange estimation method in Hulun Lake at daytime and nighttime from June to September during 2001–2018, and analyze the climate factors that affect its changes. This study mapped surface energy budget in order to better understand spatial and temporal variations in Hulun Lake. Studying the heat flux of the Hulun Lake facilitates analysis of the heat exchange method between the air-water interface and the surrounding environment, which is crucial to understanding the hydrological cycle.

2 Materials and Methods

Such methodology means was developed upon the concept of allocating the impacts to which the lakes are ex-

posed. They have been described by Alcântara et al (2010), including longwave, shortwave radiation, sensible heat flux and latent heat flux in the region. Wind intensity, relative humidity, air temperature, atmospheric surface pressure, by which the strength of all the energy transferring through the air-water interface are determined. The budget of surface energy for the Hulun Lake was figured out employing the data about the surface temperature of lake from Moderate Resolution Imaging Spectroradiometer (MODIS) water surface temperature (WST) and the data on the wind speed, air temperature and relative humidity from reanalyzed data. In order to further explore the relationship between each heat flux and different climate factors, sensitivity analysis and correlation analysis on them were conducted to provide impact and feedback of environmental changes on heat flux. The results provide a deeper understanding of each heat flux, which can provide better insight into global climate change.

2.1 Study area

Hulun Lake (48.06°N–49.04°N, 117.01°E–117.07°E) was the biggest lake in Northeast China and the fifth biggest fresh water lake in China (Mao, 2017) (Fig. 1). The lake has a water depth about 8.0 m at maximum when the lake elevation is 545.3 m a. s. l (above sea level). The study area was in the mid-temperate continental steppe climate, and was located in the semi-arid region of the mid-high latitude temperate zone. The cli-

mate is characterized by long, cold winters, heavy winds in spring, and a short cool summer with rapid cooling in autumn. Hulun Lake freezes for a long period in the winter. Ice begins sealing the lake at the end of October and thawing generally starts at the beginning of May. The layer of ice can be as thick as over 1 m (Zhang, 1998). Owing to the large heat capacity and strong evaporation of the lake, its water surface temperature is lower than the atmospheric temperature, and temperature along the lake was lower than that of the surrounding land.

2.2 Data and Methods

2.2.1 Hydrometeorological data

The daily mean wind intensity (m/s), relative humidity (%), mean air temperature (°C), atmospheric surface pressure (mb), were from China meteorological forcing dataset (1979–2018) (Yang et al., 2018), China Meteorological Administration Land Data Assimilation System (CLDAS-V2.0) of real-time product dataset (<http://data.cma.cn/dataService/cdcindex>), GRAPES_MESO China and surrounding area numerical forecast products (<http://data.cma.cn/data/cdcdetail>), China Global Atmosphere Reanalysis Products for 40 yr (CRA-40) (<http://data.cma.cn/data/>), and National Centers for Environmental Prediction (NCEP) and National Center for Atmospheric Research (NCAR) (Kalnay et al., 1996; Dee et al., 2011). China meteorological forcing dataset (1979–2018), CMA Land Data Assimilation System

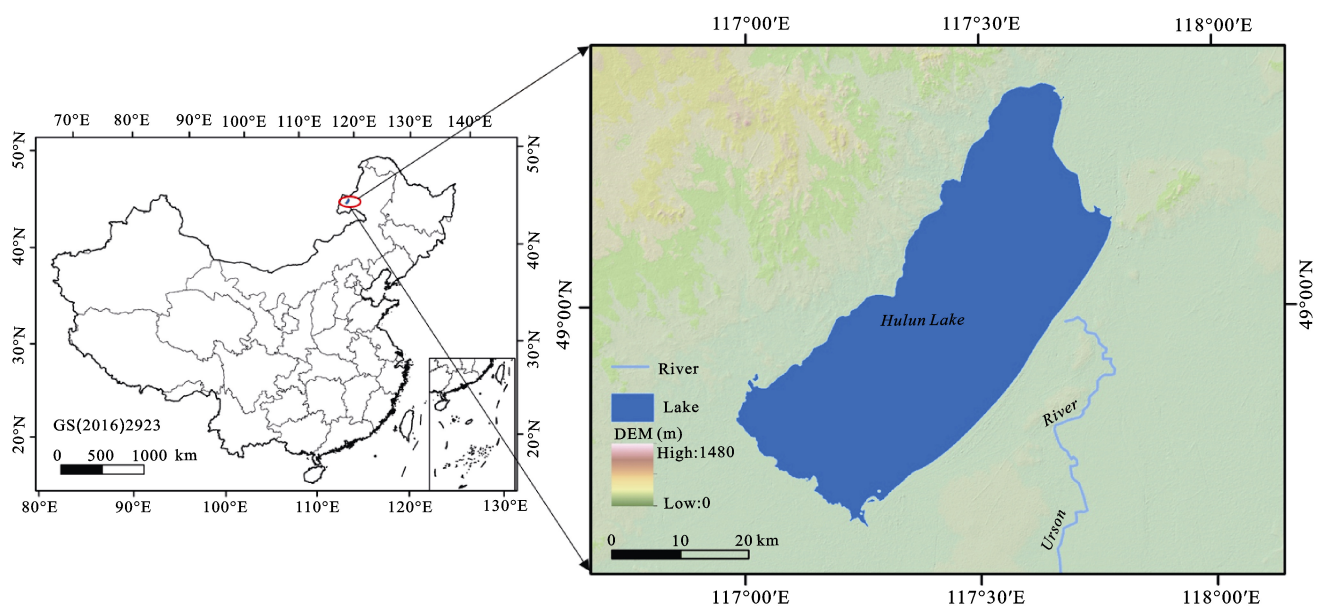


Fig. 1 Location and DEM (digital elevation model) of Hulun Lake in China

(CLDAS-V2.0) of real-time product dataset, GRAPES_MESO China and surrounding area numerical forecast products, and China Global Atmosphere Reanalysis Products for 40 yr (CRA-40) integrate conventional meteorological observation data of China Meteorological Administration, they provide high spatial and temporal resolution reanalysis data (Yang et al., 2010). NCEP/NCAR reanalysis data performs quality control and assimilation on observations from various sources to obtain a complete set of reanalysis data, which has been widely applied as an alternative long-term reference data (Hu, 1997; Goswami et al., 2004). Mean daily net shortwave radiation flux variables with China meteorological forcing dataset (1979–2018) a to better match the MODIS product, mean value of net shortwave radiation was calculated at an interval of eight days from June to September.

2.2.2 Satellite data

The MODIS water surface temperature (WST) level 21-km nominal resolution data (MOD11A2, version 5, 2015) were obtained from the National Aeronautics and Space Administration Land Processes Distributed Active Archive Center (Wan, 2008), used for Terra imagery of clear-sky MODIS from June to September from 2001 to 2018 was selected by visual inspection for a total of 286 daytime images and 286 nighttime images. The WST-MODIS data have been extensively validated for inland waters and are considered as accurate (Oesch et al., 2005). A mask of shoreline isolating the land from water was constructed employing images of Landsat 8 Operational Land Imager (OLI) to keep the warm and cold pixels isolated anomalously by the lake shoreline (Sentlinger et al., 2008). All the masked images of MODIS were verified to guarantee all the pixels to be removed in the border. The mask was constructed employing the normalized difference water index (NDWI) algorithm raised by McFeeters (1996).

This work is mainly divided into four aspects (Fig. 2): MODIS product, reanalyzed data, spatiotemporal analysis of heat flux, and relationship between heat flux and climate factors.

2.2.3 Surface energy budget

The budget of surface energy for the Hulun Lake was figured out employing the data about the surface temperature of lake from MODIS WST and the data on the wind speed, air temperature and relative humidity from reanalyzed data. Researching the energy exchanging

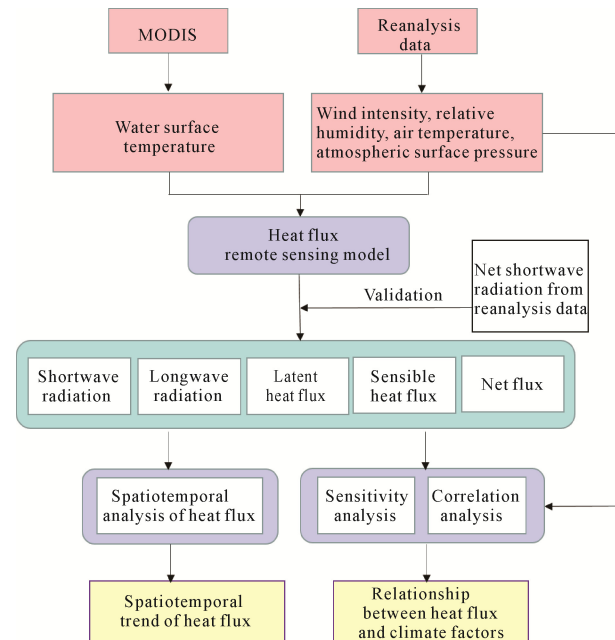


Fig. 2 The flowchart of this study

from a lake to the atmosphere is crucial for learning the operation of an aquatic mechanism and its feedback to the variations in the climatic and environmental conditions (Bonnet et al., 2000). The exchanges of heating through the surface of water was counted by the means described by Henderson-Sellers (Henderson-Sellers, 1986) as below:

$$\phi_N = \phi_s(1 - A) - (\phi_{ri} + \phi_{sf} + \phi_{lr}) \quad (1)$$

where ϕ_N is the surface heat flux balance, ϕ_s is the incident shortwave, A is the albedo of water (0.07), Cogley (1979) suggests that an annual global mean value of 0.07 would be appropriate, and this value is averaged over both cloudy and cloud-free conditions. ϕ_{ri} is the longwave radiation flux, ϕ_{sf} is sensible heat flux, and ϕ_{lr} is latent heat flux. The variables listed in Eq. (1) are expressed in unit of W/m^2 .

The incident shortwave radiation ϕ_s was calculated using the following equation (Schladow et al., 2004):

$$\phi_s = a_1 \times \phi_0 \times (\sin d)^{b_1} (1 - 0.65C^2) \quad (2)$$

where $a_1 = 0.79$ and $b_1 = 1.15$ are the parameters of calibration decided by comparing with the data of radiometer, $\phi_0 = 1390 W/m^2$ is the solar constant, d is the solar zenith angle, and C is the cloud cover index figured out employing the empirical relation of Reed (1977).

The net longwave (LW) radiation (ϕ_{li}), corresponding to the difference between outgoing flux and incoming flux ($LW\uparrow\downarrow = LW\uparrow - LW\downarrow$), was calculated as (Lowe, 1977):

$$\phi_{li} = \varepsilon \times \sigma \times T_s^4 \times (0.39 - 0.05E_a^{0.5}) \times (1 - \lambda \times C) + 4\varepsilon \times \sigma \times T_s^3 \times (T_s - T_a) \quad (3)$$

where ε is the water emissivity of thermal infrared (0.97), σ is the constant of Stefan-Boltzmann, T_s is water surface temperature (WST, °C), T_a is surface air temperature (°C), λ is the Reed's (Reed, 1977) correction factor (0.8), and E_a the partial pressure of vapor (mb). The latter parameter was derived from the equation:

$$E_a = 0.6108 \times R \times H \times \exp\left(\frac{17.27T_a}{T_a + 237.3}\right) \quad (4)$$

where R is relative humidity and H the saturation vapor pressure which was calculated using the polynomial approximation by Lowe (1977). The nonradiative energy term accounts for the sensible and latent heat fluxes. The sensible heat flux was estimated as follows (Large et al., 1997):

$$\phi_{sf} = \rho_a \times C_p \times C_H \times U \times (T_s - T_a) \quad (5)$$

where ϕ_{sf} is the sensible heat flux (W/m^2), ρ_a is the density of air ($1.2 \text{ kg}/m^3$), C_p is the specific heat capacity of air ($1.005 \times 10^3 \text{ J}/(\text{kg}\cdot\text{K})$), C_H is the coefficient of turbulent exchange (1.1×10^{-3}), and U is surface wind speed (m/s).

The latent heat flux was calculated as follows (Large et al., 1997):

$$\phi_{lf} = \rho_a \times C_E \times L \times U \times (E_{sat} \times T_s - R \times H \times E_{sat} \times T_a) \times \frac{0.622}{P_a} \quad (6)$$

where ϕ_{lf} is the latent heat flux (W/m^2), C_E is the coefficient of turbulent exchange (1.1×10^{-3}), L is the vaporization of latent heat ($2.501 \times 10^6 \text{ J}/\text{kg}$), E_{sat} is the saturation vapor pressure and P_a is the atmospheric surface pressure (mb). Energy exchange also occurred through precipitation, and biological and chemical reactions in the body of water, as well as in the exchanging from Kinetic to the energy of thermal. Nevertheless, those energy terms were regarded less to be deleted.

2.2.4 Sensitivity analysis

In order to analyze the sensitivity of different influenc-

ing factors, we used a method, the basic principle of the one-variable-at-a-time approach (OAT) for sensitivity analysis is to calculate the small changes (such as 10% increase or decrease) caused by each parameter near its best estimate. The rate of change in the model output, the absolute value of the rate of change represents the sensitivity of the parameter (Cho et al., 2016). The OAT method is the most frequently applied technique in the modeling literature (Saltelli and Annoni, 2010; Sun et al., 2012). Output variations are evaluated with respect to fractional change in one input parameter, while the other parameters are held constant. In this study, each input parameter was perturbed by +10% relative to its reference value. The sensitivity of the j th input parameter is calculated by:

$$S_j = \frac{\phi_{(j+\Delta j)} - \phi_j}{\phi_j} \quad (7)$$

where j is meteorological elements, Δj is the perturbed input parameter, ϕ_j is heat flux before changing each meteorological factor. Past studies have shown that omitting these components from the energy budget of lakes does not significantly affect the results (Bolsenga, 1975; Sturrock et al., 1992; Winter et al., 2003). The latent and sensible heating fluxes were figured out for night time and day time employing the surface water temperature of monthly mean produced from the products of MODIS.

3 Results

3.1 Validation of net shortwave radiation

We used the method described by Henderson-Sellers to estimate the net shortwave radiation. To evaluate the reliability of estimated net shortwave radiation, a comparison with daily net shortwave radiation variables with China meteorological forcing dataset (1979–2018) was conducted. Mean value of net shortwave radiation was calculated at an interval of eight days from June to September. The value of net shortwave radiation in China meteorological forcing dataset (1979–2018) was used to validate our estimation. The coefficient relating the estimated net shortwave radiation to the reanalysis data was $R^2 = 0.81$ ($n = 16$) (Fig. 3). The root means square errors ($RMSE$) was $55.13 \text{ W}/m^2$. Because of the net shortwave radiation mainly depends on the solar altitude angle and has a dynamic process within a day.

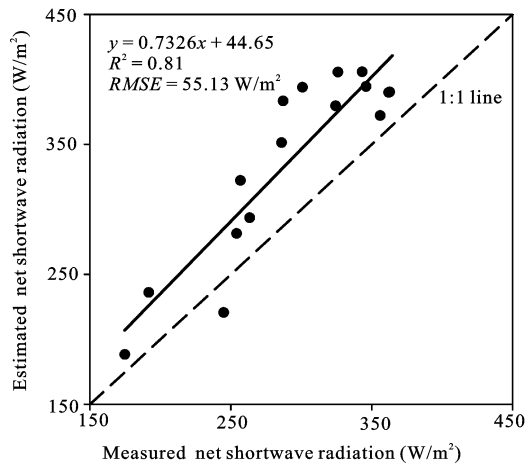


Fig. 3 Evaluation of the estimated net shortwave radiation over Hulun Lake in 2015

And our estimated net shortwave radiation was based on MODIS LST products. The transit time of MODIS was about 11:30 am. At this moment, the solar altitude angle was larger, and the net shortwave radiation value was also larger. Based on long-term meteorological observation records, Alcântara et al. (2010) estimated the shortwave of the Itumbiara reservoir by using the same method as ours. The simple regression between their estimated and measured shortwave shows a $R^2 = 0.72$ (Alcântara et al., 2010) in Itumbiara reservoir. Thus, our used the method might fit more to the data set that we used China meteorological forcing dataset (1979–2018). Our results could be acceptable under this circumstance.

3.2 Annual surface energy budget

The relative errors in net radiation indicate that the balance of the surface heat flux was affected mainly as the regions with radiation of longwave and sensible heat flux were pushed by the variations among the water and air temperatures, whereas flux of latent was affected by the intensity of wind (Henderson-Sellers, 1986). We estimated the spatially-averaged monthly means over Hulun Lake of each type of radiative or heat flux, using reanalysis data and satellite data from 2001 to 2018.

3.2.1 Shortwave radiation

Shortwave radiation (ϕ_s) was the main component of the surface radiation balance, which affects the changes of other radiation components dramatically. According to Eq. (2), ϕ_s mainly dependent on the solar zenith angle,

which relies on the latitude for a given remote sensing image. It was also affected by altitude, atmospheric conditions and cloud cover. A seasonal variation showed in the mean monthly ϕ_s with a significant decline from June to September (Table 1). The highest value of ϕ_s appeared in June, which was 897.87 W/m^2 , and September was lowest value in the whole growing season. The average ϕ_s from June to September was 796 W/m^2 .

3.2.2 Net longwave radiation

The net longwave radiation (ϕ_{li}) expresses the net balance between outgoing ϕ_{li} from the lake and incoming long wave radiation from the atmosphere. Positive values indicate a loss of energy from the lake, and the greater the contrast between water and air temperatures is, the larger the flux. For net long wave radiation, a loss of energy occurred throughout the growing season in both daytime and nighttime. The difference between lake and atmospheric temperatures decreased in daytime, and therefore, daytime losses were the greatest (Fig. 4). Daytime ϕ_{li} increased from June to August (139.99 W/m^2), and decreased into September (128.28 W/m^2). ϕ_{li} at nighttime declined from June to July (159.57 W/m^2), and rise up by the August (162.85 W/m^2). It then declined again slightly in September (157.57 W/m^2).

3.2.3 Sensible heat flux

A negative sensible heat flux (ϕ_{sf}) occurs when surface loses heat by convective and advective processes, and flux was positive when surface gains heat (Fig. 5). For daytime, ϕ_{sf} was positive for all months during the investigation period, which gradually increases from June to September. Lowest value occurred in June (4.73 W/m^2), although September was a month of typical heat gain, with highest value was reached 6.17 W/m^2 . At nighttime, ϕ_{sf} was negative for all months of the growing season. There was no obvious change trend in ϕ_{sf} . The lowest value appeared in September (-30.27 W/m^2). The highest value occurred in July (-21.06 W/m^2) that was due to advection caused by relatively high wind intensity (4.1 m/s).

Table 1 Estimated mean monthly shortwave radiation (ϕ_s) over Hulun Lake (W/m^2)

	Jun.	Jul.	Aug.	Sept.
Shortwave radiation	897.86	877.01	785.18	622.96

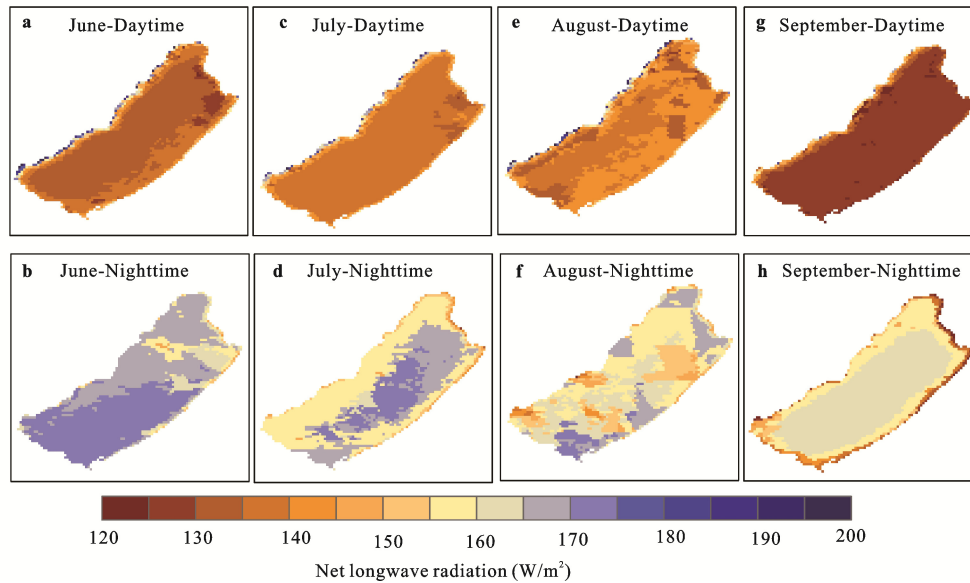


Fig. 4 Estimated monthly mean net longwave radiation over Hulun Lake from June to September during daytime and nighttime

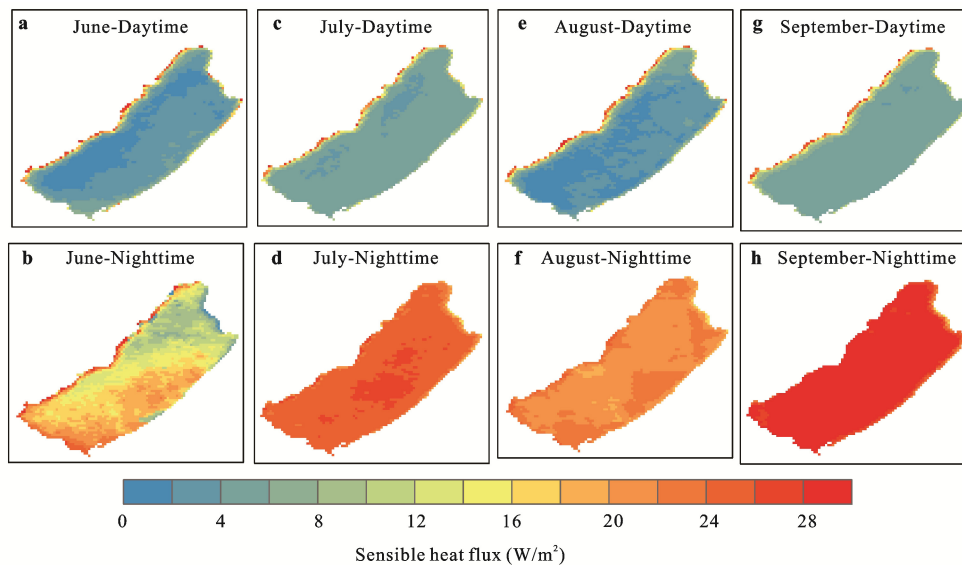


Fig. 5 Estimated monthly mean sensible heat flux over Hulun Lake from June to September during daytime and nighttime

3.2.4 Latent heat flux

The monthly latent heat flux (ϕ_f) over Hulun Lake was positive (Fig. 6), explaining a heat gain at daytime and nighttime from June to September. In general, trend of ϕ_f was identical to that of ϕ_s for both daytime and nighttime. As air temperature decreased, the same trend goes with ϕ_f from June to September. According to the Fig. 6, the ϕ_f was related to atmospheric saturation difference. In June, atmospheric temperature was at its peak, saturation difference was large, the evaporation capacity was strong,

and ϕ_f was large. However, in September, temperature was relatively low, saturation difference is small, the evaporation capacity is relatively weak, and ϕ_f was small. ϕ_f was forcefully affected by diurnal variations in boundary seam of atmosphere, stabilized conditions was needed for its enhancement (Lerman et al., 1995). As per the Zhu and Lofgren (Lofgren and Zhu, 2000), an active ϕ_f normally takes place where atmosphere was stable above the body of water, with small amount of mixed turbulent in the boundary seam of atmosphere.

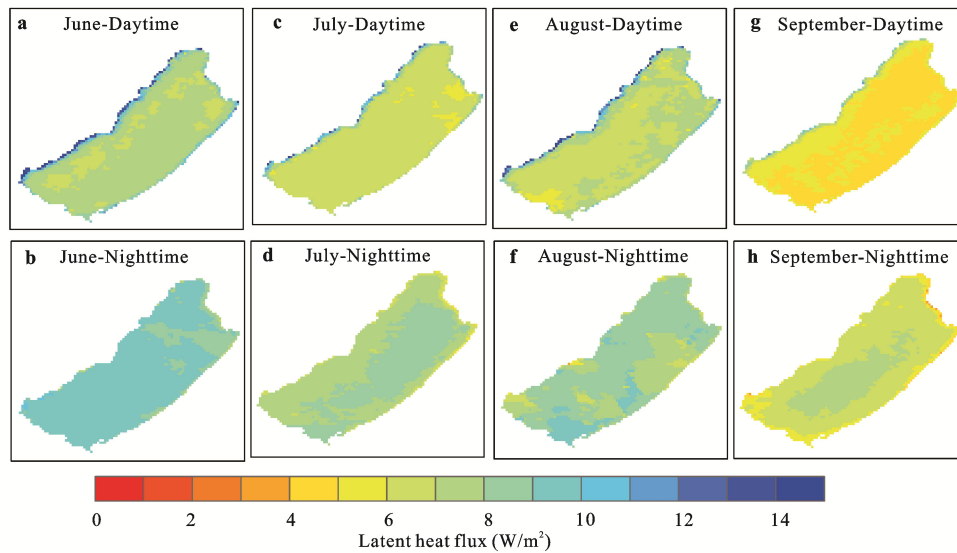


Fig. 6 Estimated monthly mean latent heat flux (ϕ_l) over Hulun Lake from June to September during daytime and nighttime

3.2.5 Net flux

Daytime flux was always positive, corresponding to a source of energy (Fig. 7), whereas ϕ_N during nighttime always corresponded to a loss of energy from lake (negative values) because of the cessation of ϕ_S . This result occurred because the loss terms (back long wave radiation, sensible heat flux, and latent heat flux) were usually

not counterbalanced by the source terms (shortwave and atmospheric long wave radiation). At daytime, ϕ_N was nearly similar to that of ϕ_S . ϕ_N steadily decreased from June (686.31 W/m^2) until September (439.76 W/m^2). Nighttime, absolute value of maximum of ϕ_N appeared in June (-202.82 W/m^2). The value of daytime ϕ_N was always greater than the absolute value of nighttime ϕ_N .

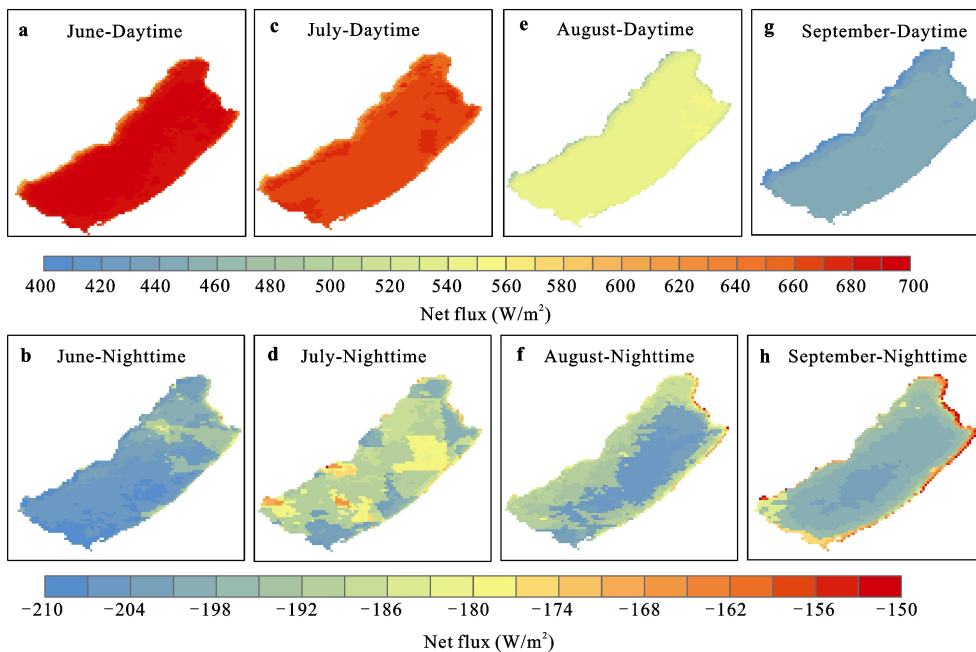


Fig. 7 Estimated monthly mean net flux (ϕ_N) over Hulun Lake from June to September during daytime and nighttime

3.3 Inter-annual surface energy budget

As showed in Fig. 8, the inter-annual trend of surface energy budget was estimated by inverted heat fluxes of radiation over Hulun Lake during the period of 2001–2018. According to Eq. (2), shortwave radiation (ϕ_s) was dependent on the solar zenith angle, which relies in turn on the latitude for a given remote sensing image. So the ϕ_s in one specific inland lake were determined by Julian date of year.

The trends of daytime and nighttime longwave radiation (ϕ_{li}) were similar (Fig. 8a). It has a significant growth trend from 2001 to 2018 during daytime ($P < 0.01$). The perennial average at daytime was 136.34 W/m^2 , whereas the range of ϕ_{li} was $128.08\text{--}146.12 \text{ W/m}^2$. The trend in different time periods was not completely consistent. It increased from 2001 to 2005 and then decreased, with the minimum value occurred in 2008 (128.08 W/m^2). A slight rise of ϕ_{li} occurred from 2008 to 2018. Moreover, the nighttime ϕ_{li} displayed a similar trend of that at daytime. The multi-year average of ϕ_{li} at nighttime was 164.81 W/m^2 . However the range of ϕ_{li} was $151.4\text{--}170.96 \text{ W/m}^2$ at nighttime.

The value of sensible flux (ϕ_{sf}) was much smaller than the value of ϕ_{li} . But trends at the daytime and nighttime for ϕ_{sf} were similar for ϕ_{li} (Fig. 8b). The ϕ_{sf} showed a significant increasing trend from 2001 to 2018 ($P < 0.01$). The average ϕ_{sf} during the daytime was 5.37 W/m^2 , while the ϕ_{sf} range was $2.27\text{--}11.2 \text{ W/m}^2$. The ϕ_{sf} decreased from 2001 to 2007, reached its minimum at 2007 (2.27 W/m^2), but then increased from 2007 to 2010. It increased again slightly in 2011 until 2014.

Similarly, the average of ϕ_{sf} during nighttime was -24.58 W/m^2 . Inter-annual range was from -14.87 to -34.35 W/m^2 . The nighttime ϕ_{sf} decreased from fluctuations in 2001 to 2010, but increased to 2011 (-34.37 W/m^2), where it reached a maximum, and then decreased to 2018.

Latent heat flux (ϕ_{lf}) had the same as ϕ_{sf} , and ϕ_{lf} showed a clear growth trend from 2001 to 2018 ($P < 0.01$) (Fig. 8c). During daytime, the average value of ϕ_{lf} was 6.64 W/m^2 , and ϕ_{lf} range was $4.3\text{--}9.8 \text{ W/m}^2$. The ϕ_{lf} increased from 2001 to 2012 and then decreased during the period of 2012–2018. The tendency in ϕ_{lf} at daytime was similar with that of nighttime. The average of ϕ_{lf} during the nighttime was 7.83 W/m^2 , but the range was $4.41\text{--}11.7 \text{ W/m}^2$. The ϕ_{lf} incidence fluctuated moderately from 2001 to 2011, and a slight reduced from 2011 to 2016, then increased to 2018.

The net flux (ϕ_N) was positive at daytime, with an average value of 563.4 W/m^2 . However, night ϕ_N was negative, with an average value of -197.925 W/m^2 . Daytime ϕ_N showed a significant reduction in 2001–2018 ($P < 0.01$) (Fig. 8d). At daytime, ϕ_N increased from 2001 to 2007, and reached its maximum (575.34 W/m^2), then decreased steadily until 2018. The nighttime ϕ_N was also a slight decreased trend in 2001–2018. However, the trend of nighttime ϕ_N was similar to that at daytime, with the absolute maximums occurred in 2011 (-225.21 W/m^2) and lowest absolute values in 2008 (-170.34 W/m^2).

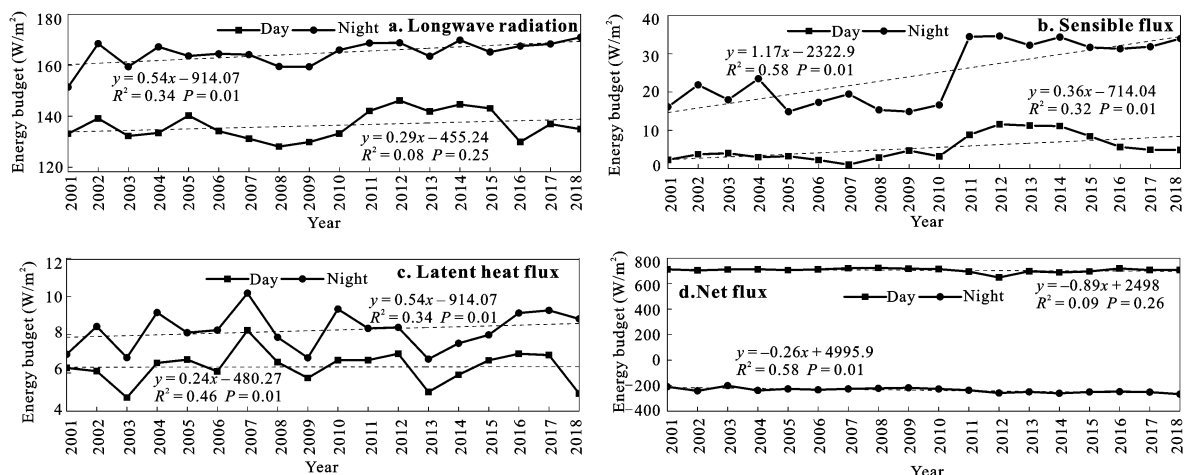


Fig. 8 Estimated components of the energy budget for daytime and nighttime during 2001–2018

4 Discussion

Lake-atmosphere interactions are an important component of climatic systems. On the one hand, a lake has an important impact on the regional climate through its own physical properties (low albedo relative to the surrounding area, large heat capacity, *etc.*) (Bonan, 1995). On the other hand, climate change alters the physical and chemical properties of the lake, which affects evaporation from the lake and energy exchange with the atmosphere (Oswald and Rouse, 2004). Lake water surface heat fluxes are affected by many different climatic factors, including air temperature, differences in saturated water vapor pressure, wind speed, *etc.* (Nordbo et al., 2011). How changes in different climate factors affect each component was an important part of our research in this study.

4.1 Relationship between longwave radiation and climate factors

We performed linear regression analysis according to Eq. (3) to determine the changed in ϕ_{ri} that were related to E_a , T_s , and T_a . The results of linear correlation analysis of several influential factors were showed in Fig. 9. The values of ϕ_{ri} were positively correlated with E_a and showed a better correlation during daytime ($R^2 = 0.35$) and nighttime ($R^2 = 0.03$) (Figs. 9e, 9f). There was a stronger correlation between ϕ_{ri} and T_s at nighttime (R^2

$R^2 = 0.11$) than there was during daytime ($R^2 = 0.03$) (Figs. 9a, 9b). However, we did detect a small correlation between ϕ_{ri} and T_a ($R^2 < 0.01$; Figs. 9c, 9d). The change in ϕ_{ri} was influenced by multiple interacting factors, so that the impact of each factor on its own was relatively small.

Our model input parameters involve various water surface parameters as well as meteorological data. The water surface parameters were obtained either directly or indirectly from satellite remote sensing inversion, and the meteorological data were obtained from weather station measurements. As a result of using several different data sources, there were many uncertainties in the input parameters applied in the model. In order to further explore the sensitivity of each flux to different climatic factors, a sensitivity analysis was used to provide crucial information regarding climate change.

For a more intuitive comparison, it is more appropriate to use the absolute value of each sensitivity coefficient for comparative analysis. The sensitivity coefficients of ϕ_{ri} and of each climate element were showed in Fig. 10. The effect of various climate elements on ϕ_{ri} during daytime and nighttime was dominated by T_s . The sensitivity coefficient was 0.1 during daytime and 0.08 at nighttime. This was followed in magnitude by the effect of T_a ; the sensitivity coefficient was 0.07 during daytime and 0.04 at nighttime. The sensitivity coefficient corresponding to E_a was small.

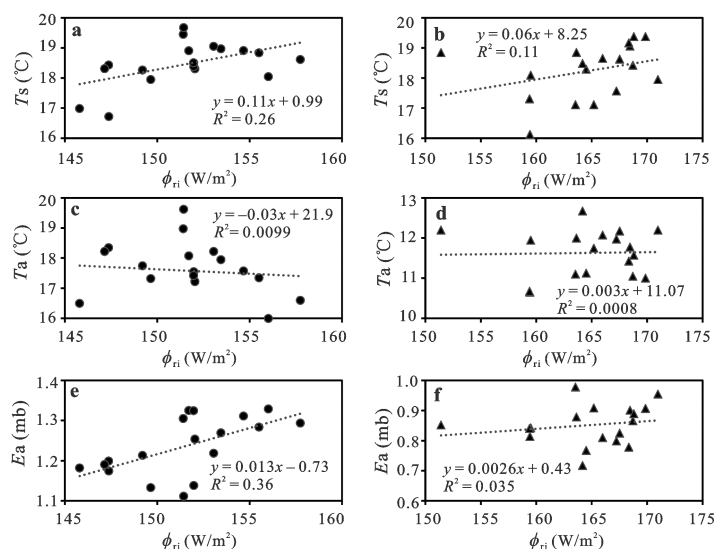


Fig. 9 Relationships between annual average net longwave radiation (ϕ_{ri}), partial vapor pressure (E_a), and water surface temperature (T_s), as estimated by Moderate Resolution Imaging Spectroradiometer water surface temperature (MODIS WST) products, and air temperature (T_a) during daytime (a; c; e) and nighttime (b; d; f) in Hulun Lake, China

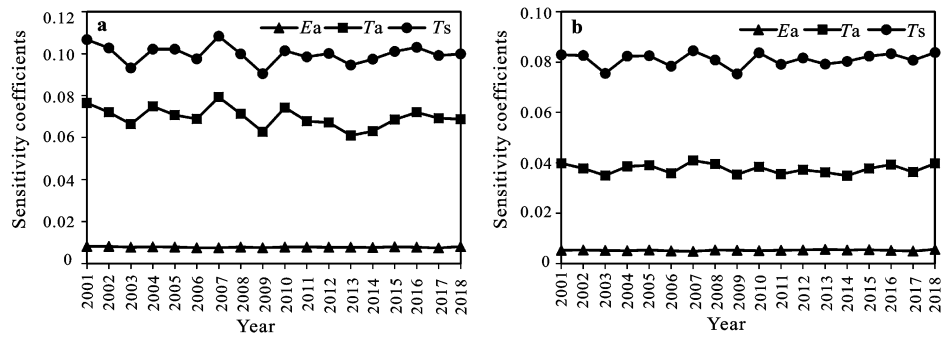


Fig. 10 Annual variation distribution of sensitive coefficients for net longwave radiation (ϕ_i) and climate factors during daytime (a) and nighttime (b) in Hulun lake, China during 2001 and 2018

4.2 Relationship between sensible heat flux and climate factors

According to Eq. (5), the exchange of ϕ_{sf} between the lake and the atmosphere was controlled mainly by T_s and T_a , as well as by U (Liu et al., 1979; Webb et al., 1980). The results were showed in Fig. 11. The values of ϕ_{sf} were positively correlated with wind speed U , indicating a good correlation (Figs. 11c, 11d); R^2 at night-

time was 0.87 and in the daytime was > 0.5). Due to solar radiation during daytime, there was a weak correlation between ϕ_{sf} and U during daytime. However, because there was no solar radiation during nighttime, the correlation between ϕ_{sf} and U was good. The best correlation was showed by ϕ_{sf} with U , and a similar conclusion was also drawn for Lake Valkea-Kotinen (Nordbo et al., 2011). However, there was a negative

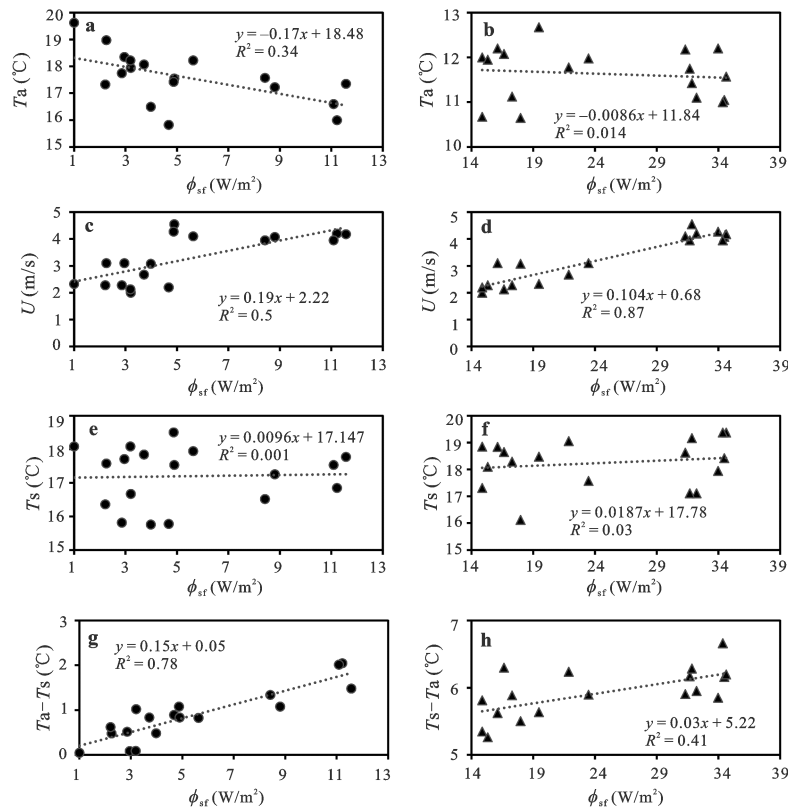


Fig. 11 Relationships between annual average sensible heat flux (ϕ_{sf}), wind speed (U), water surface temperature (T_s), and air temperature (T_a) during daytime (a; c; e; g) and nighttime (b; d; f; h) in Hulun Lake, China

correlation between ϕ_{sf} and T_a , for which R^2 during the daytime was 0.34 and at nighttime was 0.01 (Figs. 11a, 11b). The regression analysis also showed a poor correlation between ϕ_{sf} and T_s (Figs. 11e, 11f; $R^2 < 0.01$). This was because ϕ_{sf} correlated better with the difference between T_s and T_a (Figs. 11g, 11h; R^2 during daytime was 0.78 and at nighttime was 0.41).

The sensitivity coefficients of ϕ_{sf} and of each climate element were showed in Fig. 12. During daytime, the sensitivity coefficients of T_a and T_s were both greater than 2.2, indicating that they were the main climatic factors affecting ϕ_{sf} . T_a was more sensitive to ϕ_{sf} than T_s , although the sensitivity coefficients T_s and T_a both showed slightly different trends. However, the sensitivity coefficient corresponding to U was small (0.1). The sensitivity coefficients of trend for ϕ_f was different between daytime and nighttime. At nighttime, the influence of various climatic factors on ϕ_{sf} was mainly that of T_s , with a sensitivity coefficient of 0.3, followed by the effect of T_a , with a sensitivity coefficient of 0.19. The corresponding sensitivity coefficient for U was the smallest (0.13).

4.3 Relationship between latent heat flux and climate factors

According to Eq. (5), ϕ_f was related to E_a , T_s , U , and P_a . A linear correlation analysis of several climate factors was employed, and the results were showed in Fig. 13. The values of ϕ_f were significantly positively correlated with U (Figs. 13e, 13f; R^2 during daytime was 0.85 and at nighttime was 0.81). However, the values of ϕ_f were negatively, and strongly, correlated with P_a (Figs. 13g, 13h; R^2 during daytime was 0.54 and at nighttime was 0.49). The next most significant correlation was between

ϕ_f and T_s (Figs. 13a, 13b), whereas ϕ_f and E_a were the least correlated (Figs. 13c, 13d). In the study of Lake Valkea-Kotinen by Nordbo et al. (2011), the correlation between ϕ_f and E_a was higher than that between ϕ_f and U . This was due mainly to the fact that Lake Valkea-Kotinen is surrounded by forests, and the winds blowing over and around the lake are weaker. So the effect of U on ϕ_f exchange was less than that of Hulun Lake. The above results indicate that U , E_a , T_s , and T_a are the critical drivers of changes in energy, and they also demonstrate that the stability of the atmospheric boundary layer plays an important role in energy transfer involving ϕ_f (Liu et al., 2009).

The sensitivity coefficients of ϕ_f and of each climate element were showed in Fig. 14. It can be seen from the figure that the greatest effect of the various climate elements on ϕ_f during daytime and nighttime was mainly that of T_s , and the sensitivity coefficient was 0.34 during daytime and 0.2 at nighttime. The results of the sensitivity analysis of ϕ_f to climate factors during daytime and nighttime were virtually identical, and the order of the sensitivity coefficients was: $T_s > T_a > U > P_a$.

The results of the sensitivity analysis of heat flux to climatic parameters were slightly different from the correlation results. We performed sensitivity analyses based on established formulas in order to identify the most influential input parameters. The results of the correlation between heat flux and different climate elements were obtained from the correlation analysis of the meteorological data as measured by a weather station located in the proximity of the study area. As the two analyses were based on different parameters, the different methods led to completely different conclusions.

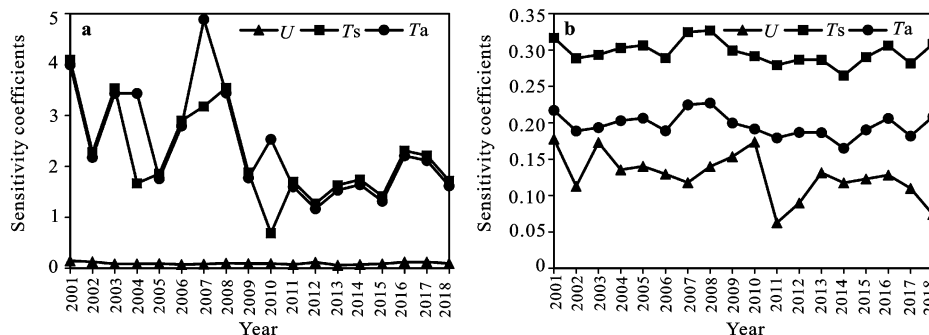


Fig. 12 Annual variation distribution of sensitive coefficients for sensible heat flux (ϕ_{sf}) and climate factors during daytime (a) and nighttime (b) in Hulun Lake, China

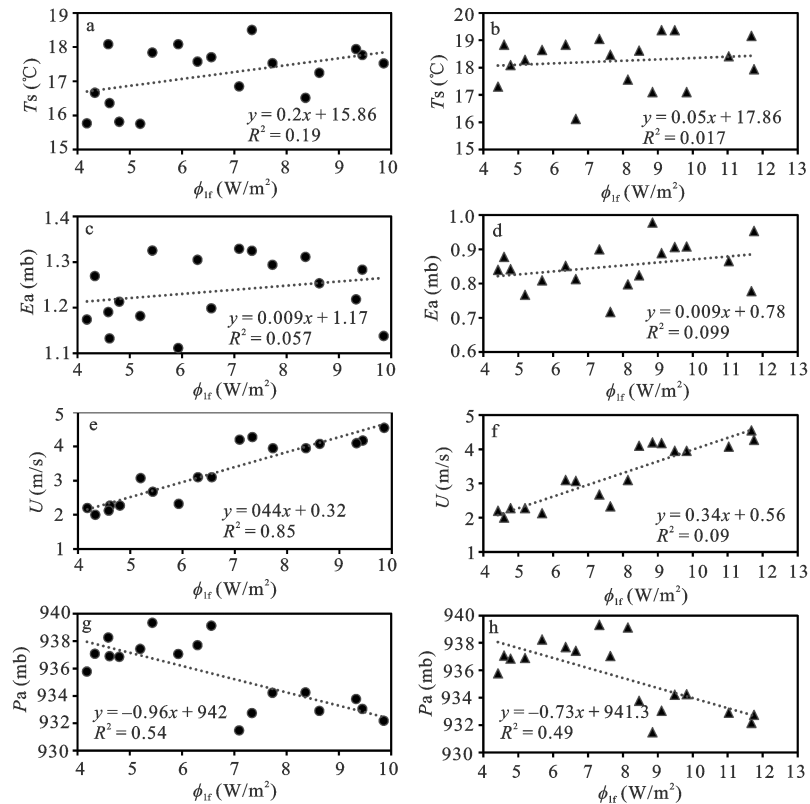


Fig. 13 Relationships between annual average latent heat flux (ϕ_{lr}), wind speed (U), partial vapor pressure (E_a), water surface temperature (T_s), and atmospheric surface pressure (P_a) during daytime (a; c; e; g) and nighttime (b; d; f; h) in Hulun Lake, China

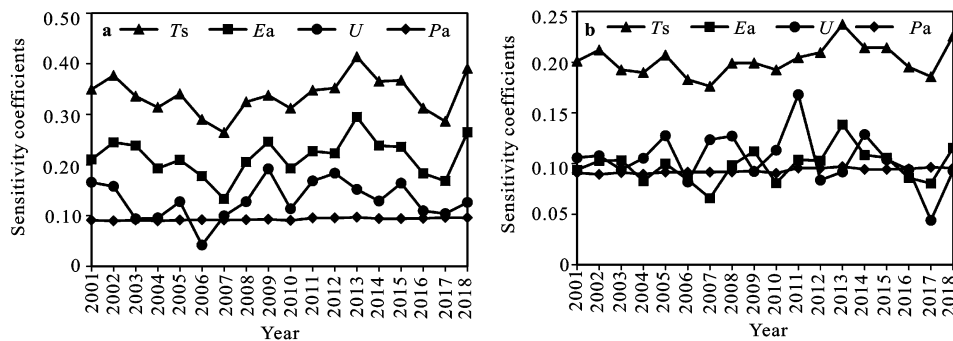


Fig. 14 Annual variation distribution of sensitive coefficients for latent heat flux (ϕ_{lr}) and climate factors during daytime (a) and nighttime (b) in Hulun Lake, China

5 Conclusions

Lake heat flux is an important part of the water balance element. It can also help us understand global climate change in a broader context. We present a set of simulation schemes for heat flux based on reanalysis data and satellite data. On the basis of this, exchange of heat across the water surface was computed to outline the temperatures of surface water and budget of surface en-

ergy to strengthen our understanding of the temporal and spatial variability of heat flux in Hulun Lake from 2001 to 2018.

We used the method which was described by Henderson-Sellers was suitable for Hulun Lake ($R^2 = 0.81$). At month scale, mean monthly shortwave radiation increased significantly from June to September. The latent heat flux decreased from June to September. Sensible heat flux increased from June to July and then decreased

to September, and net longwave radiation increased from June to August and then decreased. The efficient heating budget indicated that, in the frost free season, Hulun Lake gained heat and thus acted as a heat sink. It had maximum value in June, then steadily decreased to September. For the heat flux of daytime, a lowering pattern from the shoreline to the middle part of the lake, whereas this thermal pattern was inverted at night. On the inter-annual scale, net longwave radiation and sensible heat flux both showed a clear growth trend from 2001 to 2018 ($P < 0.01$). The net flux was positive during daytime, and was negative at nighttime. However, the daytime net flux showed a significant reduction trended in 2001–2018 ($P < 0.01$).

In the correlation analysis, the net longwave radiation and partial pressure of vapor are good correlated ($R^2 > 0.3$). However, latent heat flux and sensible heat flux were well correlated with wind speed ($R^2 > 0.7$). On the other hand, in the sensitivity analysis, water surface temperature had the highest sensitivity. Heat exchange between the air-water interfaces and the surrounding environment and mainly occur at the air-water interface.

Acknowledgement

The authors thank National Aeronautics and Space Administration (NASA) for providing MODIS LST imagery data free of charge.

References

- Bogard M J, Finlay K, Waiser M J et al., 2017. Effects of experimental nitrogen fertilization on planktonic metabolism and CO₂ flux in a hypereutrophic hardwater lake. *PLoS One*, 12(12): e0188652. doi: 10.1371/journal.pone.0188652
- Bolsenga S J, 1975. Estimating energy budget components to determine Lake Huron evaporation. *Water Resources Research*, 11(5): 661–666. doi: 10.1029/WR011i005p00661
- Bonan G B, 1995. Sensitivity of a GCM simulation to inclusion of inland water surfaces. *Journal of Climate*, 8(11): 2691–2704. doi: 10.1175/1520-0442(1995)008<2691:SOAGST>2.0.CO;2
- Bonnet M P, Poulin M, Devaux J, 2000. Numerical modeling of thermal stratification in a lake reservoir: methodology and case study. *Aquatic Sciences*, 62(2): 105–124. doi: 10.1007/s000270050001
- Chen J Q, Li N, Liu Z L et al., 2016. Area monitoring of Namco lake in summer by high-resolution TerraSAR-X spotlight mode. *Proceedings of 2016 Progress in Electromagnetic Research Symposium*. Shanghai, China: IEEE, 5140–5143. doi: 10.1109/PIERS.2016.7735858
- Cho E, Arhonditsis G B, Khim J et al., 2016. Modeling metal-sediment interaction processes: parameter sensitivity assessment and uncertainty analysis. *Environmental Modelling & Software*, 80: 159–174. doi: 10.1016/j.envsoft.2016.02.026
- Cole J J, Caraco N F, Kling G W et al., 1994. Carbon dioxide supersaturation in the surface waters of lakes. *Science*, 265(5178): 1568–1570. doi: 10.1126/science.265.5178.1568
- de Alcântara E H, Stech J L, Lorenzetti J A et al., 2011. Time series analysis of water surface temperature and heat flux components in the Itumbiara Reservoir (GO), Brazil. *Acta Limnologica Brasiliensia*, 23(3): 245–259. doi: 10.1590/S2179-975X2012005000002
- Dee D P, Uppala S M, Simmons A J et al., 2011. The ERA—Interim reanalysis: configuration and performance of the data assimilation system. *Quarterly Journal of the Royal Meteorological Society*, 137(656): 553–597. doi: 10.1002/qj.828
- Edinger J E, Duttweiler D W, Geyer J C, 1968. The response of water temperatures to meteorological conditions. *Water Resources Research*, 4(5): 1137–1143. doi: 10.1029/WR004i005p01137
- Goswami B N, 2004. Interdecadal change in potential predictability of the Indian summer monsoon. *Geophysical Research Letters*, 31(16): L16208. doi: 10.1029/2004GL020337
- Hébert I, Dunlop E S, 2020. Temperature response in the physiology and growth of lake trout strains stocked in the Laurentian Great Lakes. *Journal of Great Lakes Research*, 46(2): 366–375. doi: 10.1016/j.jglr.2020.01.012
- Henderson-Sellers B, 1986. Calculating the surface energy balance for lake and reservoir modeling: a review. *Reviews of Geophysics*, 24(3): 625–649. doi: 10.1029/RG024i003p00625
- Hodges J L, Saylor J R, Kaye N B, 2016. A functional form for the diurnal variation of lake surface temperature on lake Hartwell, northwestern south Carolina. *IEEE Journal of Selected Topics in Applied Earth Observations and Remote Sensing*, 9(8): 3564–3577. doi: 10.1109/JSTARS.2016.2555798
- Hu Z Z, 1997. Interdecadal variability of summer climate over East Asia and its association with 500 hPa height and global sea surface temperature. *Journal of Geophysical Research*, 102(D16): 19403–19412. doi: 10.1029/97JD01052
- Huttunen J T, Alm J, Liikanen A et al., 2003. Fluxes of methane, carbon dioxide and nitrous oxide in boreal lakes and potential anthropogenic effects on the aquatic greenhouse gas emissions. *Chemosphere*, 52(3): 609–621. doi: 10.1016/S0045-6535(03)00243-1
- Kalnay E, Kanamitsu M, Kistler R et al., 1996. The NCEP/NCAR 40-year reanalysis project. *Bulletin of the American meteorological Society*, 77(3): 437–472. doi: 10.1175/1520-0477(1996)077<0437:TNYRP>2.0.CO;2
- Large W G, Danabasoglu G, Doney S C et al., 1997. Sensitivity to surface forcing and boundary layer mixing in a global ocean model: annual-mean climatology. *Journal of Physical Oceanography*, 27(11): 2418–2447. doi: 10.1175/1520-0485(1997)

- 027<2418:STSFAB>2.0.CO;2
- Lerman A, Imboden D M, Gat J R, 1995. Physics and Chemistry of Lakes. 2nd ed. Berlin, Germany: Springer. doi: 10.1007/978-3-642-85132-2
- Li Chong, Ma Wei, Ye Baisheng et al., 2006. Estimation of water evaporation and water balance in Ungauged Hulun Lake. *Journal of China Hydrology*, 26(5): 41–44. (in Chinese)
- Liu H P, Zhang Y, Liu S H et al., 2009. Eddy covariance measurements of surface energy budget and evaporation in a cool season over southern open water in Mississippi. *Journal of Geophysical Research*, 114(D4): D04110. doi: 10.1029/2008JD010891
- Liu W T, Katsaros K B, Businger J A, 1979. Bulk parameterization of air-sea exchanges of heat and water vapor including the molecular constraints at the interface. *Journal of the Atmospheric Sciences*, 36(9): 1722–1735. doi: 10.1175/1520-0469(1979)036<1722:BPOASE>2.0.CO;2
- Lofgren B M, Zhu Y C, 2000. Surface energy fluxes on the Great Lakes based on satellite-observed surface temperatures 1992 to 1995. *Journal of Great Lakes Research*, 26(2): 305–314. doi: 10.1016/S0380-1330(00)70694-0
- Lowe P R, 1977. An approximating polynomial for the computation of saturation vapor pressure. *Journal of Applied Meteorology*, 16(1): 100–103. doi: 10.1175/1520-0450(1977)016<0100:AAPFTC>2.0.CO;2
- Mao J H, 2017. Study on the temporal and spatial pattern of achatherum splendens community in Hulun Lake area. *Proceedings of 2017 International Conference on Society Science*. Atlantis Press. doi: 10.2991/icos-17.2017.13
- McFeeters S K, 1996. The use of the Normalized Difference Water Index (NDWI) in the delineation of open water features. *International Journal of Remote Sensing*, 17(7): 1425–1432. doi: 10.1080/01431169608948714
- Nordbo A, Launiainen S, Mammarella I et al., 2011. LongA, Launnergy flux measurements and energy balance over a small boreal lake using eddy covariance technique. *Journal of Geophysical Research*, 116(D2): D02119. doi: 10.1029/2010JD014542
- Oesch D C, Jaquet J M, Hauser A et al., 2005. Lake surface water temperature retrieval using advanced very high resolution radiometer and Moderate Resolution Imaging Spectroradiometer data: validation and feasibility study. *Journal of Geophysical Research*, 110(C12): C12014. doi: 10.1029/2004JC002857
- Oswald C J, Rouse W R, 2004. Thermal characteristics and energy balance of various-size Canadian Shield lakes in the Mackenzie River Basin. *Journal of Hydrometeorology*, 5(1): 129–144. doi: 10.1175/1525-7541(2004)005<0129:TCAEBO>2.0.CO;2
- Pour H K, Choulga M, Eerola K et al., 2017. Towards improved objective analysis of lake surface water temperature in a NWP model: preliminary assessment of statistical properties. *Tellus A: Dynamic Meteorology and Oceanography*, 69(1): 1313025. doi: 10.1080/16000870.2017.1313025
- Qiao B J, Zhu L P, Wang J B et al., 2019. Estimation of lake water storage and changes based on bathymetric data and altimetry data and the association with climate change in the central Tibetan Plateau. *Journal of Hydrology*, 578: 124052. doi: 10.1016/j.jhydrol.2019.124052
- Reed R K, 1977. On estimating insolation over the ocean. *Journal of Physical Oceanography*, 7(3): 482–485. doi: 10.1175/1520-0485(1977)007<0482:OEIOTO>2.0.CO;2
- Saltelli A, Annoni P, 2010. How to avoid a perfunctory sensitivity analysis. *Environmental Modelling & Software*, 25(12): 1508–1517. doi: 10.1016/j.envsoft.2010.04.012
- Schladow S G, Pálmarsson S Ó, Steissberg T E et al., 2004. An extraordinary upwelling event in a deep thermally stratified lake. *Geophysical Research Letters*, 31(15): L15504. doi: 10.1029/2004GL020392
- Sentlinger G I, Hook S J, Laval B, 2008. Sub-pixel water temperature estimation from thermal-infrared imagery using vectorized lake features. *Remote Sensing of Environment*, 112(4): 1678–1688. doi: 10.1016/j.rse.2007.08.019
- Sharaf N, Fadel A, Bresciani M et al., 2019. Lake surface temperature retrieval from Landsat-8 and retrospective analysis in Karaoun Reservoir, Lebanon. *Journal of Applied Remote Sensing*, 13(4): 044505. doi: 10.1117/1.JRS.13.044505
- Sturrock A M, Winter T C, Rosenberry D O, 1992. Energy budget evaporation from Williams Lake: a closed lake in north central Minnesota. *Water Resources Research*, 28(6): 1605–1617. doi: 10.1029/92WR00553
- Steissberg T E, Hook S J, Schladow S G et al., 2005. Characterizing partial upwellings and surface circulation at Lake Tahoe, California–Nevada, USA with thermal infrared images. *Remote sensing of environment*, 99(1–2): 2–15. doi: 10.1029/2005GL022912
- Sun X Y, Newham L T H, Croke B F W et al., 2012. Three complementary methods for sensitivity analysis of a water quality model. *Environmental Modelling & Software*, 37: 19–29. doi: 10.1016/j.envsoft.2012.04.010
- Viridis S G P, Soodcharoen N, Lugliè A et al., 2020. Estimation of satellite-derived lake water surface temperatures in the western Mediterranean: integrating multi-source, multi-resolution imagery and a long-term field dataset using a time series approach. *Science of the Total Environment*, 707: 135567. doi: 10.1016/j.scitotenv.2019.135567
- Wan Z M, 2008. New refinements and validation of the MODIS land-surface temperature/emissivity products. *Remote Sensing of Environment*, 112(1): 59–74. doi: 10.1016/j.rse.2006.06.026
- Wang Y L, Wang L, Cheng J L et al., 2019. Recognizing crucial aquatic factors influencing greenhouse gas emissions in the eutrophication zone of Taihu Lake, China. *Sustainability*, 11(19): 5160. doi: 10.3390/su11195160
- Wang Yajuan, Mi Wenbao, Wang Li et al., 2010. Study on sustainable utilization of Ningxia Xinghai Lake wetland based on assessment of water environment pollution. *Journal of Agricultural Sciences*, 31(4): 46–49. (in Chinese)
- Webb E K, Pearman G I, Leuning R, 1980. Correction of flux measurements for density effects due to heat and water vapour transfer. *Quarterly Journal of the Royal Meteorological Society*, 106(447): 85–100. doi: 10.1002/qj.49710644707

- Winter T C, Buso D C, Rosenberry D O et al., 2003. Evaporation determined by the energy-budget method for Mirror Lake, New Hampshire. *Limnology and Oceanography*, 48(3): 995–1009. doi: 10.4319/lo.2003.48.3.0995
- Woolway R I, Jones I D, Maberly S C et al., 2016. Diel surface temperature range scales with lake size. *PLoS One*, 11(3), e0152466. doi: 10.1371/journal.pone.0152466
- Xu L Y, Zhang P A, Fang X J et al., 2009. Multi-range fusion technique using multi-channel monitoring SST. *Proceedings of the 2009 5th International Conference on Semantics, Knowledge and Grid*. Zhuhai, China: IEEE, 49–53. doi: 10.1109/SKG.2009.35
- Yang Kun, He Jie, 2018. China meteorological forcing dataset (1979–2018). National Tibetan Plateau Data Center, doi: 10.11888/AtmosphericPhysics.tpe.249369.file
- Yang K, Yu Z Y, Luo Y et al., 2019. SpatialK, Yu Z Y, Luo Y et al., 2019. Spogical forcing dataseand its driving factors in Yunnan-Guizhou Plateau. *Water Resources Research*, 55(6): 4688es Re. doi: 10.1029/2019WR025316
- Zhang G Q, Xie H J, Gao Y, 2011. Seasonal snow cover variations in the Nam Co basin of Tibetan Plateau using MODIS data. In: *Proceedings of the 2011 19th International Conference on Geoinformatics*. Shanghai, China: IEEE, 1–4. doi: 10.1109/GeoInformatics.2011.5980902
- Zhang Z B, 1998. *Annals of the Lake (Sequel 1)*. Hohhot: Inner Mongolia Cultural Publishing House.